TECHNICAL MEMORANDUM

772

A lightning parameterization for the ECMWF model

Philippe Lopez

Research Department

To be submitted to the Monthly Weather Review

January 2016

European Centre for Medium-Range Weather Forecasts
Europäisches Zentrum für mittelfristige Wettervorhersage
Centre européen pour les prévisions météorologiques à moyen terme

Series: ECMWF Technical Memoranda

A full list of ECMWF Publications can be found on our web site under:
http://www.ecmwf.int/en/research/publications

Contact: library@ecmwf.int

European Centre for Medium-Range Weather Forecasts
Shinfield Park, Reading, RG2 9AX, England

Abstract

A new parameterization able to diagnose lightning flash densities is proposed for the ECMWF Integrated Forecasting System, including its tangent-linear and adjoint versions. Lightning densities are expressed as a function of hydrometeors contents, convective available potential energy and cloud base height output by the convection scheme. Potential future applications range from the computation of NO_x emissions by lightning in the chemistry model, severe convection forecasting and data assimilation. In this study, a decade-long experiment is used to calibrate the global annual mean flash density against the LIS/OTD climatological value. On the seasonal and continental scales, the new parameterization is shown to agree rather well with the LIS/OTD observations. In forecast mode, output lightning densities are found to be almost independent of the horizontal resolution used in the model. Decade-long experiments also show that the new parameterization gives better results overall than the main existing lightning parameterizations designed for global models. Sensitivity experiments using its adjoint version are also performed to assess its potential for the future assimilation of lightning observations in the ECMWF 4D-Var system.

1 Introduction

Lightning is an important component of the Earth's atmosphere in several respects. It is predominantly observed over tropical land areas but also midlatitude continents during the warm season, where it can trigger devastating fires in vegetated regions, disrupt power lines, cause serious damage to buildings and can even be occasionally life threatening. Lightning is also known to be a source of NO_x gases which can in turn affect the ozone field in the troposphere and the stratosphere and thus influence the Earth's climate (e.g. Schumann and Huntrieser 2007).

Even though our knowledge of the many processes involved in the triggering of lightning is still very incomplete, the physical interactions between hydrometeors is today recognized as the dominant source of convective storm electrification. Two categories of processes, namely the non-inductive and the inductive mechanisms, are commonly considered to explain electric charge separation within clouds. First, the non-inductive mechanism corresponds to the charge transfer occurring during the collisions between rimed graupel/hail and snow/cloud-ice particles. This mechanism is thought to be responsible for the initial electrification of the storm and it is also a major contributor to its subsequent intensification or maintenance. A reversal in the polarity of the charge gained by the precipitating particles is usually observed around $-10°$C (positive/negative charge for warmer/colder temperatures), although liquid water amount and graupel/hail riming rate may also play a role in this reversal. On the other hand, the inductive mechanism requires the pre-existence of a relatively strong electric field (i.e. well above its fair-weather value of around 100 V m^{-1}) in order to polarize hydrometeors. It may therefore occur only after the storm has been sufficiently electrified through the non-inductive mechanism. The inductive charge transfer is most efficient during the rebounding collisions between frozen precipitation particles (ice, graupel or hail) and supercooled liquid droplets. Overall, charge separation leads to the typical charge distribution shown in Figure 1, with positive charges in the upper part of the storm (cloud ice), negative charges between roughly $-25°$C and $-10°$C (graupel) and a thinner positively charged layer from cloud base up to roughly $-10°$C. Lightning discharges occur everytime the electric field that builds up from charge separation reaches a threshold in the order of 200 to 600 kV m^{-1}. The charge deposited by each lightning discharge is highly variable, with typical values ranging from 10 to 100 C (Maggio *et al.* 2009). Several authors (e.g. Williams *et al.* 2002, Stolz *et al.* 2015) have suggested that higher contents of aerosols which act as cloud condensation nuclei might modulate lightning occurrence by reducing the efficiency of the warm rain coalescence process and by producing smaller cloud droplets that are more readily lifted to the charge separation region, well above the freezing level. Even though this "aerosol hypothe-

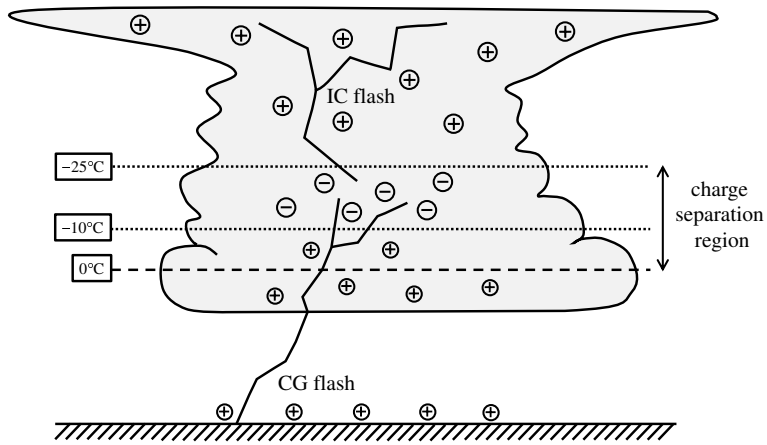

FIGURE 1: Idealized electric charge distribution in a mature thunderstorm. "CG" and "IC" stand for cloud-to-ground and intra-/inter-cloud lightning, respectively.

sis" has been put forward as a possible explanation for the much weaker lightning activity observed over oceans as well as for the significantly lower activity over the Amazon region compared to Central Africa (Williams ans Sátori 2004), its importance remains to be clearly demonstrated on the global scale.

Lightning flashes can be categorized as either cloud-to-ground (CG), intra-cloud or inter-cloud, the two latter categories being usually merged together and labelled as IC discharges. The climatological ratio of IC with respect to total (IC+CG) lightning typically varies between 35% and 90% (MacGorman and Rust 1998) depending on the geographical location. A large uncertainty remains as regards what governs the spatial and temporal fluctuations of this ratio (Boccippio *et al.* 2001). A further distinction between positive and negative CG flashes is based on the sign of the charge inside the region from which lightning leaders originate. Positive ground flashes usually account for less than 10% of the total number of CG flashes.

From an observational standpoint, over the past decades, ground-based lightning detection networks have been developed throughout the world, some of them dedicated to specific regions (NLDN, Orville and Huffines 2001; LINET, Betz *et al.* 2009; Zeus, Chronis and Anagnostou 2003), others offering a global coverage (GLDN, Said *et al.* 2010; ATDnet, Anderson and Klugmann 2014; WWLLN, Rodger *et al.* 2006). A list of acronyms can be found in Appendix 1. These networks of sensors are designed to detect the electromagnetic radiation (the so-called "sferics") emitted by lightning discharges (mainly CG) at Very-Low-Frequency (VLF) or Low-Frequency (LF). As a result of the propagation of electromagnetic waves inside the ionospheric waveguide, the detection range of such sensor can reach several thousand kilometres. Another type of sensors that work at Very-High-Frequency (VHF) is used in lightning mapping arrays that can provide detailed information on the three-dimensional characteristics of individual flashes over limited geographical domains (Goodman *et al.* 2005). In addition, observations also became available from polar-orbiting satellites in the 1990s, first from OTD (1995-2000; Christian *et al.* 2003) and then from TRMM-LIS (1997-2015; Christian *et al.* 1999). These two space-borne imagers were both designed to measure the near-infrared (777 nm) radiation emitted from both IC and CG lightning flashes with a spatial resolution of around 9 km for OTD and 4 km for LIS.

As far as the development of lightning parameterizations for numerical weather prediction applications is concerned, the direct link between charge separation mechanisms and collisions between hydrometeors led many modellers to relate storm electrical activity and therefore lightning discharges to the characteristics (e.g. amount, fall velocity) of hydrometeors (graupel, hail, cloud ice, snow and supercooled liquid

water droplets) as well as to the intensity of the convection itself (e.g. updraught velocity, convective available potential energy). Based on Vonnegut's (1963) theory on the geometry of the charged regions and on his scaling assumptions for the convective cloud characteristics (updraught velocity), Price and Rind (1994) proposed simple formulae to estimate both total and cloud-to-ground lightning flash rates over land and ocean from the convective cloud top heights simulated by their global circulation model. Boccippio (2002) showed that Price and Rind's parameterization for ocean locations implied somewhat inconsistent assumptions, leading to a clear underestimation of flash densities over sea. Using LIS observations, Boccippio (2002) proposed revised parameterizations, still based on the convective cloud top heights only, yet without demonstrating their applicability in an operational context. Grewe (2001) designed a slightly more elaborate formulation by combining simulated cloud top height with the convective mass flux diagnosed by the ECHAM4 global circulation model. This latter parameterization was validated by Kurz and Grewe (2002). As an alternative, Allen and Pickering (2002) computed CG flash rates using a polynomial function of convective precipitation. Romps *et al.* (2014) used a simple formulation based on precipitation and convective available potential energy to predict the trend in lightning activity over the United States as a result of climate change. Dahl *et al.* (2011) related the storm-scale effects of charging and discharging processes on lightning flash rates to the amount of graupel predicted by their limited-area model. Finney *et al.* (2014) parameterized lightning flash rate as a linear function of the upward cloud ice mass flux at 440 hPa, emphasizing the importance of explicitly including ice to better describe the non-inductive charging mechanism. Much more complex electrification schemes able to account for the time evolution of the space charge/electrical field resulting from the interaction between various types of hydrometeors were also developed for cloud-resolving models at horizontal resolutions of a few hundred metres (e.g. Barthe *et al.* 2005, Fierro *et al.* 2013). The parameterizations proposed by Mansell *et al.* 2002 and Barthe *et al.* 2005 even included an explicit simulation of the propagation of individual lightning flashes.

The implementation of such detailed and computationally expensive parameterizations in the current version of the ECMWF global model would be irrelevant given its still rather crude representation of microphysical processes and its relatively coarse horizontal resolution (currently 16 km in operations). Therefore, the purpose of the present study is to introduce a new, relatively simple, lightning parameterization capable of estimating total lightning flash densities from diagnostic fields of the ECMWF forecast model and to investigate potential future applications. Section 2 provides a brief introduction to the forecast model used in this study while section 3 describes the new lightning parameterization. LIS/OTD observations are presented in section 4, which are then used in section 5 to calibrate and validate the lightning parameterization outputs in multi-annual 80-km resolution simulations as well as in short-range model integrations at higher resolutions. Section 6 reports on sensitivity computations performed using the adjoint version of the new lightning parameterization. Conclusions and prospects are given in section 7.

2 Forecast model

The new lightning parameterization has been developed and tested in the framework of the ECMWF global Integrated Forecasting System (IFS), described at http://old.ecmwf.int/ifsdocs/. In particular, the new parameterization uses outputs from the convective mass-flux scheme of the IFS (Bechtold *et al.* 2014). It should be emphasized that in the latter scheme convective cloud condensate and precipitation amounts are purely diagnostic quantities and that no information on graupel/hail amounts is available as standard. All experiments presented in this paper were performed using recent versions of the ECMWF model (namely either 41r2 or 42r1). Besides, adjoint sensitivity experiments presented in section 6 used

all linearized physical parameterizations described in Janisková and Lopez (2013), which were specially designed for the ECMWF four-dimensional variational (4D-Var) data assimilation system (Courtier it et al. 1994; Rabier it et al. 2000).

3 Lightning parameterization

The new parameterization of total lightning flash densities proposed here involves quantities that are diagnosed from the ECMWF convection scheme, namely:

- the convective available potential energy (CAPE; in J kg^{-1}),
- the vertical profile of the frozen precipitation convective flux (P_f; in kg m^{-2} s^{-1}),
- the profile of cloud condensate amount within the convective updraught (q_{cond}; in kg kg^{-1}),
- the convective cloud base height (z_{base}; in km).

First, the respective amounts of graupel (q_{graup}; in kg kg^{-1}) and snow (q_{snow}; in kg kg^{-1}) are diagnosed from the following partitioning of P_f for each model vertical level:

$$q_{graup} = \beta \frac{P_f}{\overline{\rho}\, V_{graup}} \tag{1}$$

$$q_{snow} = (1-\beta) \frac{P_f}{\overline{\rho}\, V_{snow}} \tag{2}$$

where $\overline{\rho}$ denotes the environmental air density (kg m^{-3}) and V_{graup} and V_{snow} are typical fall speeds for graupel and snow set to 3.0 and 0.5 m s^{-1}, respectively. The dimensionless coefficient β is set equal to 0.7 over land and 0.45 over sea to account for the observed lower graupel contents over oceans (Takahashi 2006).

Then a quantity, Q_R, assumed to be proportional to the charging rate resulting from the collisions between graupel and other types of hydrometeors inside the charge separation region, is empirically computed as

$$Q_R = \int_{z_0}^{z_{-25}} q_{graup} \left(q_{cond} + q_{snow}\right) \overline{\rho} dz \tag{3}$$

where z_0 and z_{-25} are the heights of the 0°C and −25°C isotherms, respectively.

Convective available potential energy is diagnosed from the vertical integral of the buoyancy profile as

$$CAPE = \int_{z_{LFC}}^{z_{w=0}} \max\left(g \frac{T_v^u - \overline{T_v}}{\overline{T_v}}, 0\right) dz \tag{4}$$

where g is the constant of gravity and T_v^u and $\overline{T_v}$ denote the virtual temperatures in the updraught and in the environment, respectively. Vertical integration is performed between the level of free convection, z_{LFC}, and the level where the updraught vertical velocity vanishes, $z_{w=0}$. One should note that entrainment is included in the computation of T_v^u, but precipitation water loading is disregarded.

Finally, the total (IC and CG) lightning flash density (f_T; in flashes km^{-2} day^{-1}), is determined as

$$f_T = \alpha\, Q_R \sqrt{CAPE}\, \min\left(z_{base}, 1.8\right)^2 \tag{5}$$

where α is a constant obtained after calibration against the LIS/OTD climatology (see section 4), which is set to 36.6706 here. The dependence of f_T on $\sqrt{CAPE}$ is included to account for the observed correlation

of lightning frequency with updraught vertical velocity. The term in z_{base} can be seen as a proxy for the horizontal extent of the convective ascent (Williams and Stanfill 2002), which is assumed to increase with z_{base}^2, before becoming constant once z_{base} exceeds 1.8 km.

In addition, the tangent-linear and adjoint versions of the lightning parameterization have been coded and tested. This will allow future studies of the feasibility of assimilating lightning observations in the ECMWF 4D-Var system. In the present work, the adjoint code was used in adjoint sensitivity experiments presented in section 6.

4 Lightning observations

The OTD instrument on board the low-earth-orbit (710 km altitude) MicroLab-1 satellite (OV-1) consisted of a telescope optimized to identify lightning during day and night in the 777-nm near-infrared wavelength. OTD was active from April 1995 to March 2000 and observed all geographical regions between 75°N and 75°S with a resolution of about 9 km over a 1300 km field of view. During the day, the signal due to lightning flashes can be disentangled from the background illumination by applying various methods aiming at maximizing the signal-to-noise ratio (Christian *et al.* 1989). A detection efficiency between 37 and 52% depending on local time (minimum around noon) is assumed in the estimation of the actual lightning flash densities from OTD (Cecil *et al.* 2014a). It should be noted that the detection efficiency of OTD is halved over the South Atlantic Anomaly near eastern South America. Indeed, the lower altitude of the Van Allen radiation belt over this region implies that the OTD signal-to-noise ratio increases due to higher levels of geomagnetic radiation. More details about OTD can be found in Christian *et al.* (2003).

Similar observations were collected between 1997 and 2015 using LIS (Christian *et al.* 1999) on board the low-earth-orbit TRMM satellite. Pixel resolution of LIS was about 4 km, while the coverage was limited to 38°N-38°S, with a field of view of about 600 km. The detection efficiency of LIS is assumed to vary between 69 and 88%, which is higher than for OTD (Cecil *et al.* 2014a). Besides, one should note that LIS was less affected by the South Atlantic Anomaly than OTD because of its lower altitude (around 400 km).

Cecil *et al.* (2014a) recently extended the original 5-year OTD lightning climatology of Christian *et al.* (2003) into a LIS/OTD climatology over the period 1995-2010. It should be emphasized that given the rather small sampling in both time and space of LIS and OTD due to their low-earth orbits, regional statistics based on these observations are only meaningful on seasonal or longer timescales. Figure 2 shows a global map of the total viewing time of the combined LIS and OTD instruments over the 1995-2010 period. This total duration varies between 60 and 500 hours with a rather zonal structure, as expected, except over the South Atlantic Anomaly where OTD data availability was reduced. Figure 2 indicates that the uncertainty in the LIS/OTD climatology is likely to be higher poleward of 38° than in the tropics as only five years of OTD data (with poorer detection efficiency than LIS) were available for building the climatology over the former regions.

The 0.5-degree resolution LIS/OTD monthly lightning climatology used in this study was retrieved from the file ftp://ghrc.nsstc.nasa.gov/pub/lis/climatology/HRMC/data/LISOTD_HRMC_V2.3.2014.hdf (Cecil *et al.* 2014b).

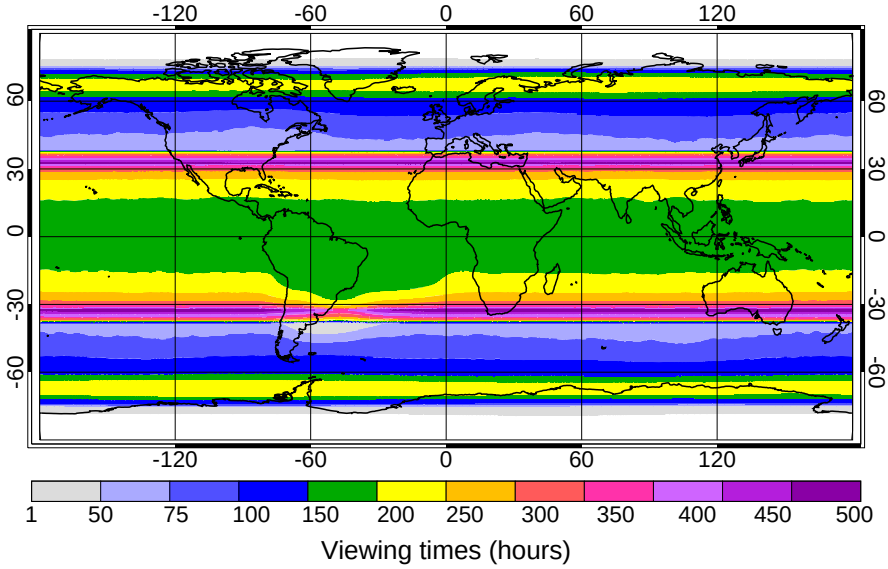

FIGURE 2: Total LIS/OTD viewing time (in hours) in the 1995-2010 lightning flash density climatology of Cecil *et al.* (2014a, 2014b).

5 Validation of the lightning parameterization

One should keep in mind that in the following validation of the simulated lightning activity against observations, it is not only the performance of the new lightning parameterization which is evaluated, but also the ability of the forecast model to properly simulate convective activity.

5.1 80-km multi-year simulations

The new lightning parameterization has been tested in an ensemble of ten 12-month-long experiments with the ECMWF model (version 41r2). These model integrations were performed using a T255 spectral truncation (approx. 80 km resolution) and 137 vertical levels. The ten year-long simulations were initialized from the ECMWF ERA-Interim reanalyses valid at 0000 UTC 1 January for the years 1999 to 2008. It should be mentioned that the coefficient α appearing in Eq. (5) was tuned so that the simulated 1999-2008 *global annual mean* lightning flash density would match the corresponding LIS/OTD 1995-2010 climatological value. This calibration on the global scale was assumed to be acceptable despite the incomplete overlap between the periods of the two datasets.

Figure 3 and Fig. 4 display the annual and seasonal mean geographical distribution of simulated lightning flash densities against the LIS/OTD 1995-2010 climatology described in section 4. Note that the plot scale spans almost two orders of magnitude. First, as a result of the calibration mentioned earlier, one can verify that the simulated global mean annual flash rate exactly matches the LIS/OTD value of 46.5 flashes s^{-1}, as expected. This mean flash rate is equivalent to the mean flash density of 2.88 flashes km^{-2} $year^{-1}$ reported at the top of each panel in Fig. 3. Secondly, one can see that the sharp contrast observed between land and ocean throughout the year is well reproduced in the simulations. The simulated annual mean flash densities over land and ocean are equal to 7.71 and 0.92 flashes km^{-2} $year^{-1}$, respectively, which is in good agreement with the corresponding LIS/OTD values of 7.69 and 0.93. Figure 3 also indicates that the model agrees fairly well with the observations over

most regions of the globe on the annual timescale, especially over land where most of the lightning is recorded. The most active regions in Africa, South America, India, Southeast Asia, Australia and North America are rather well captured in the simulations. However, the worlwide maximum value (up to 70 flashes km^{-2} year^{-1}) found over the Congo Basin in LIS/OTD data is underestimated in the model and located slightly to the north. This might indicate a deficiency in the lightning parameterization/forecast model but could also be the result of an overestimation of extreme lightning conditions in the LIS/OTD climatology, as suggested in Beirle *et al.* 2014. The observed weaker activity over Europe is also reasonably well represented in the model, but an underestimation is visible on both sides of the central Ural mountains (60°E). A slight underestimation can also be identified in the simulations compared to LIS/OTD over some ocean regions located near continents and over which thunderstorms are likely to propagate from land. This is for instance the case over the coastal waters bathing Central America, as well as over the Mediterranean Sea, in the Bay of Bengal and the South China Sea. The use of fixed separate values of β for land and ocean in Eq. (1) and Eq. (2), which turned out to be necessary to properly simulate the global contrast between land and ocean, might provide a partial explanation for the latter imperfection. By contrast, the slightly stronger lightning activity observed by LIS/OTD over sea around 30° of latitude off the east coasts of South America, South Africa, Australia and the United States can also be found in the simulations.

On the seasonal timescale, Fig. 4 shows that the overall cycle of lightning activity throughout the year is usually well simulated over all continents compared to LIS/OTD. On the regional scale however, the model tends to overestimate lightning flash densities over the Sahel region in spring and summer (Fig. 4.c-f) and to underestimate it over the Congo Basin throughout the year, as already mentioned. Besides, in the autumn (Fig. 4.g-h), the maximum of lightning activity over the Mediterranean Sea is absent in the simulations (probably because of the lower value of β), while the peak in the number of flashes over the Amazon Basin is underestimated by up to 50%. It is therefore not so surprising that the autumn is the season which exhibits by far the largest model−LIS/OTD difference in mean global standard deviation (6.36 versus 8.06 flashes km^{-2} year^{-1}, respectively). Other seasons agree much better.

As a complement, Fig. 5 displays a comparison of mean lightning flash densities from the simulations and from LIS/OTD observations for each season and the whole year. The pairs of curves are usually in good agreement, with only a systematic underestimation in the simulations over the Americas during the second half of the year (Fig. 5.c-d).

As a further evaluation, the new parameterization was also compared with existing lightning parameterizations from the literature, with the same experimental set-up described earlier in this section. The parameterizations that were tested are those from Price and Rind (1994; "PR94"), Allen and Pickering (2002; "AP02"), Grewe *et al.* (2001; "GR01") and Meijer *et al.* (2001; "MJ01") , which were all designed for global atmospheric circulation models. One should stress that the lightning flash densities obtained from each parameterization were scaled to match the global mean annual values from LIS/OTD to ensure a fairer comparison. As a summary of the results, Fig. 6 displays a Taylor diagram of the global annual mean performance of each parameterization against the LIS/OTD climatology in terms of correlation and standard deviation ratio between model and observations. Figure 6 shows that overall the new parameterization (black diamond) provides the highest correlation (0.84) and standard deviation ratio closest to the optimal unity value (black square). Both GR01 and MJ01 stand the nearest to the new parameterization, AP02 exhibits a poorer correlation with LIS/OTD (0.64), while PR94 leads to both a high standard deviation ratio (1.5) and a lower correlation (0.72). In addition, Fig. 7 displays maps of the annual mean lightning flash densities from (a) PR94, (b) AP02, (c) MJ01 and (d) GR01. The comparison of these plots with those of Fig. 3 confirms that the new lightning parameterization gives better results than the four alternative schemes. Indeed, PR94 produces too much lightning activity over the Amazon

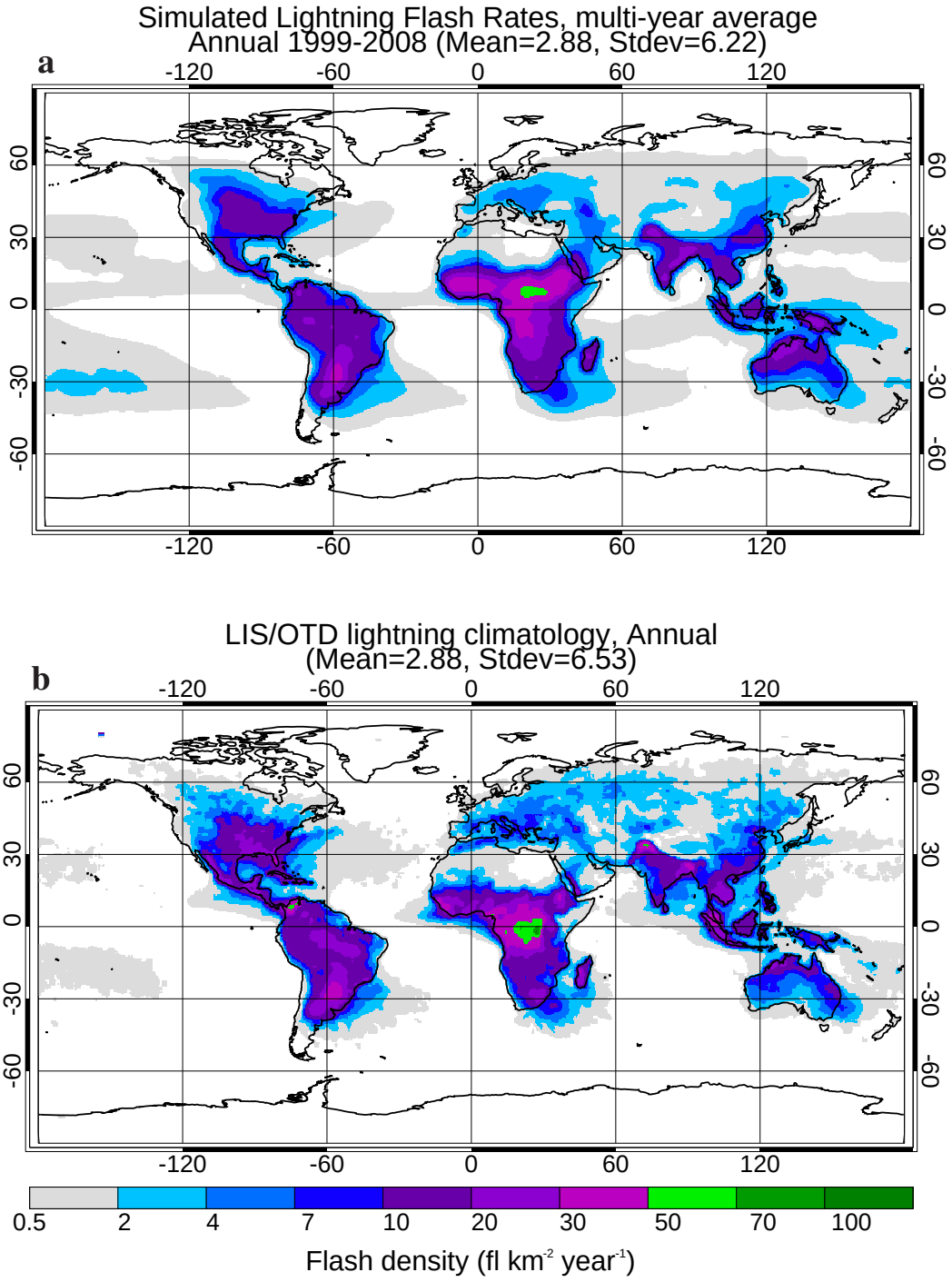

FIGURE 3: Annual mean lightning flash densities (a) from the 1999-2008 year-long 80-km global simulations and (b) from the LIS/OTD 1995-2010 climatology. Flash densities are expressed in flashes km^{-2} $year^{-1}$. Global means and standard deviations are reported at the top of each panel.

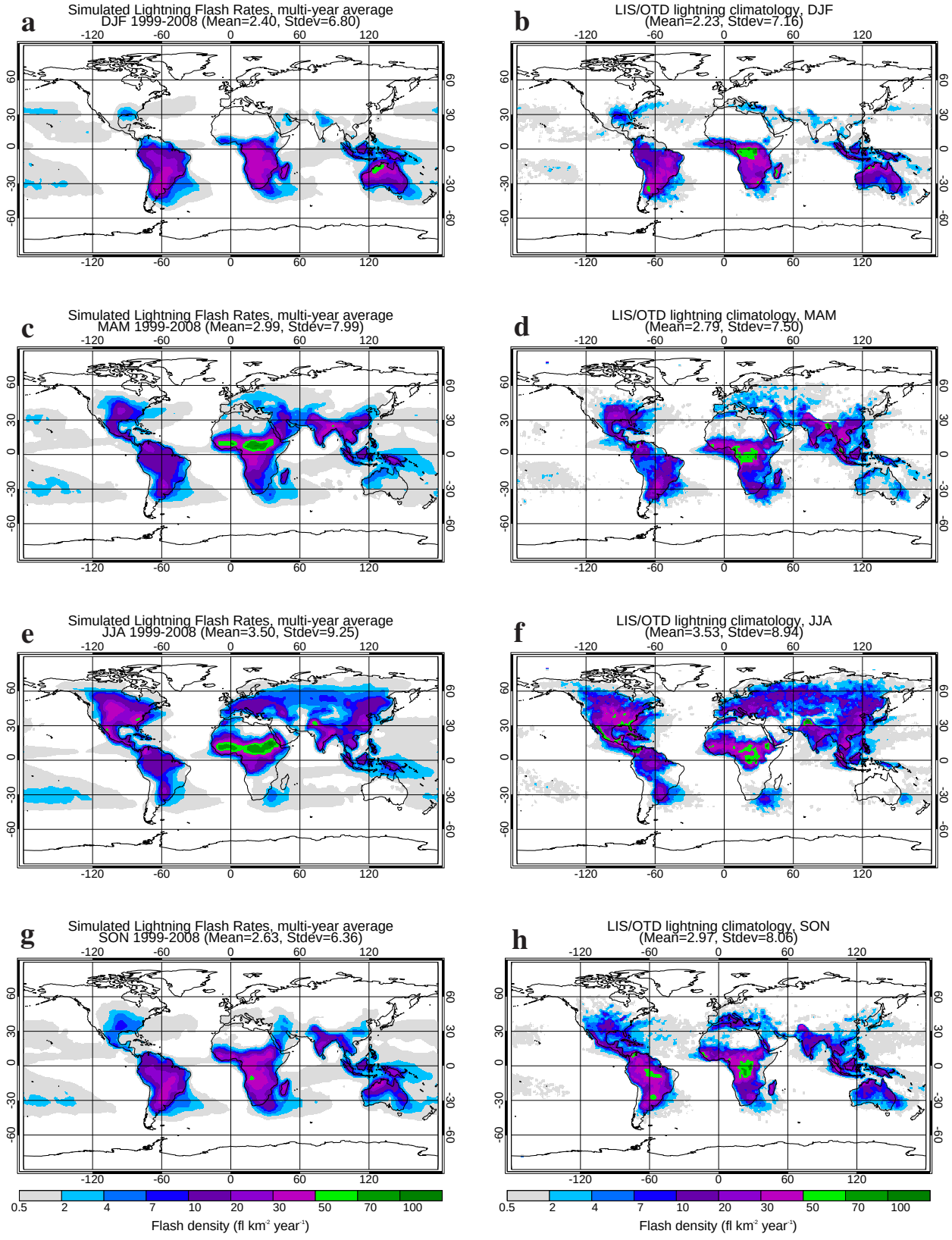

FIGURE 4: Seasonal mean lightning flash densities from the 1999-2008 year-long 80-km global simulations (left) and from the LIS/OTD 1995-2010 climatology (right): (a,b) winter, (c,d) spring, (e,f) summer and (g,h) autumn. Flash densities are expressed in flashes km^{-2} $year^{-1}$. Global means and standard deviations are reported at the top of each panel.

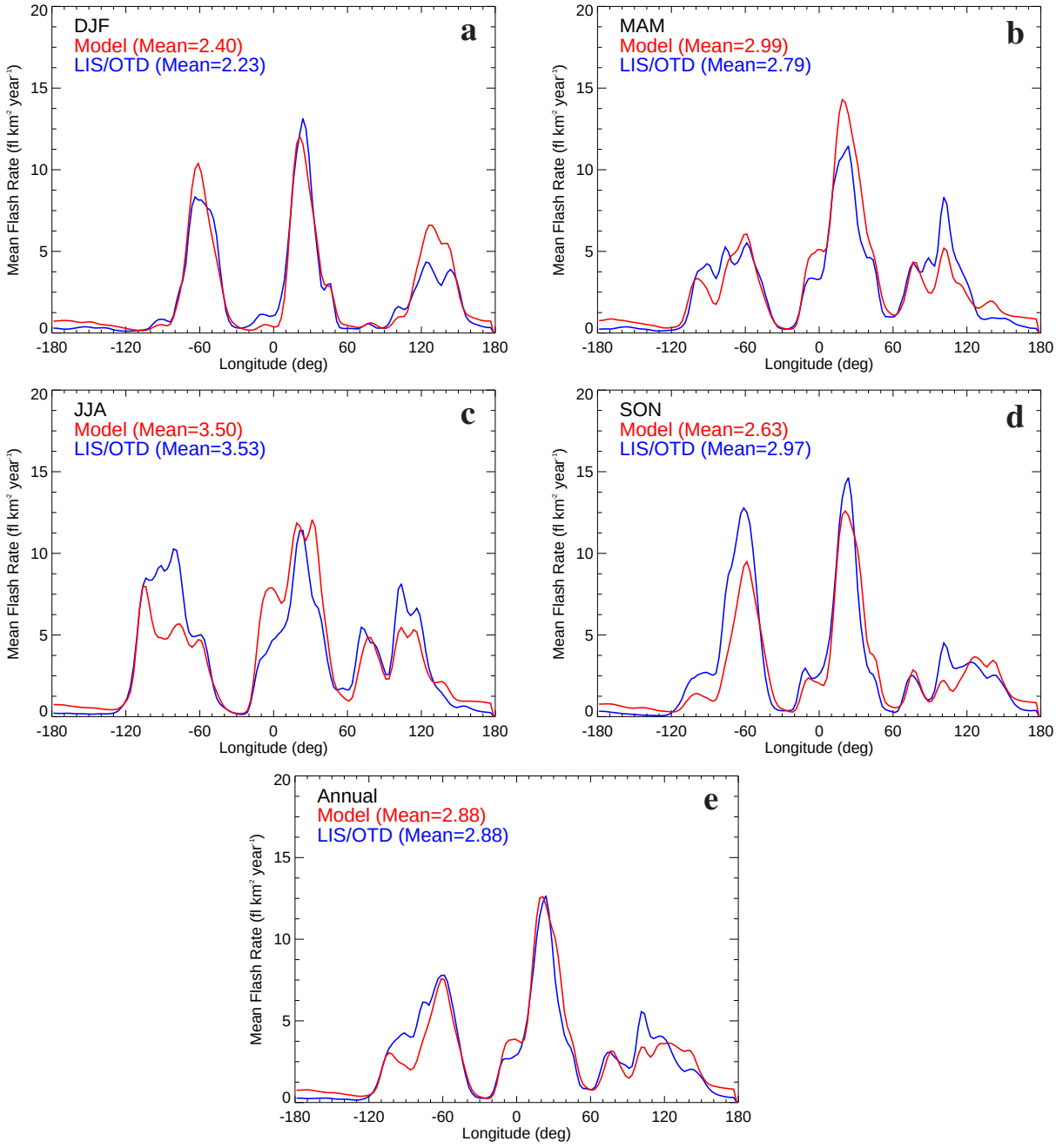

FIGURE 5: Seasonal and annual meridional mean lightning flash densities from the 1999-2008 year-long 80-km global simulations (red line) and from the LIS/OTD 1995-2010 climatology (blue line): (a) winter, (b) spring, (c) summer, (d) autumn and (e) whole year. Flash densities are expressed in flashes km^{-2} year^{-1}. The global mean for each dataset is given in parentheses in the legend.

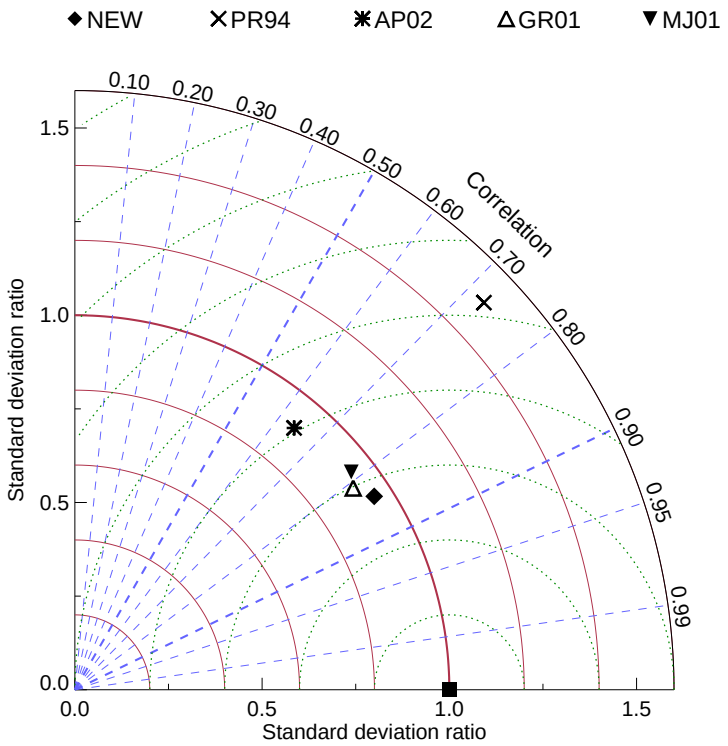

FIGURE 6: Taylor diagram showing the annual mean performance of various lightning parameterizations in 1999-2008 year-long 80-km global simulations compared to the LIS/OTD 1995-2010 climatology. In addition to the lightning parameterization introduced in this study ("NEW"), the others are Price and Rind (1994; "PR94"), Allen and Pickering (2002; "AP02"), Grewe *et al.* (2001; "GR01") and Meijer *et al.* (2001; "MJ01"). Each parameterization is displayed with a different symbol as indicated in the top legend. Correlation and standard deviation ratio between model and LIS/OTD observations are shown in the azimuthal and radial directions, respectively. A perfect match between model and observations would correspond to the black square (i.e. correlation and standard deviation ratio equal to unity).

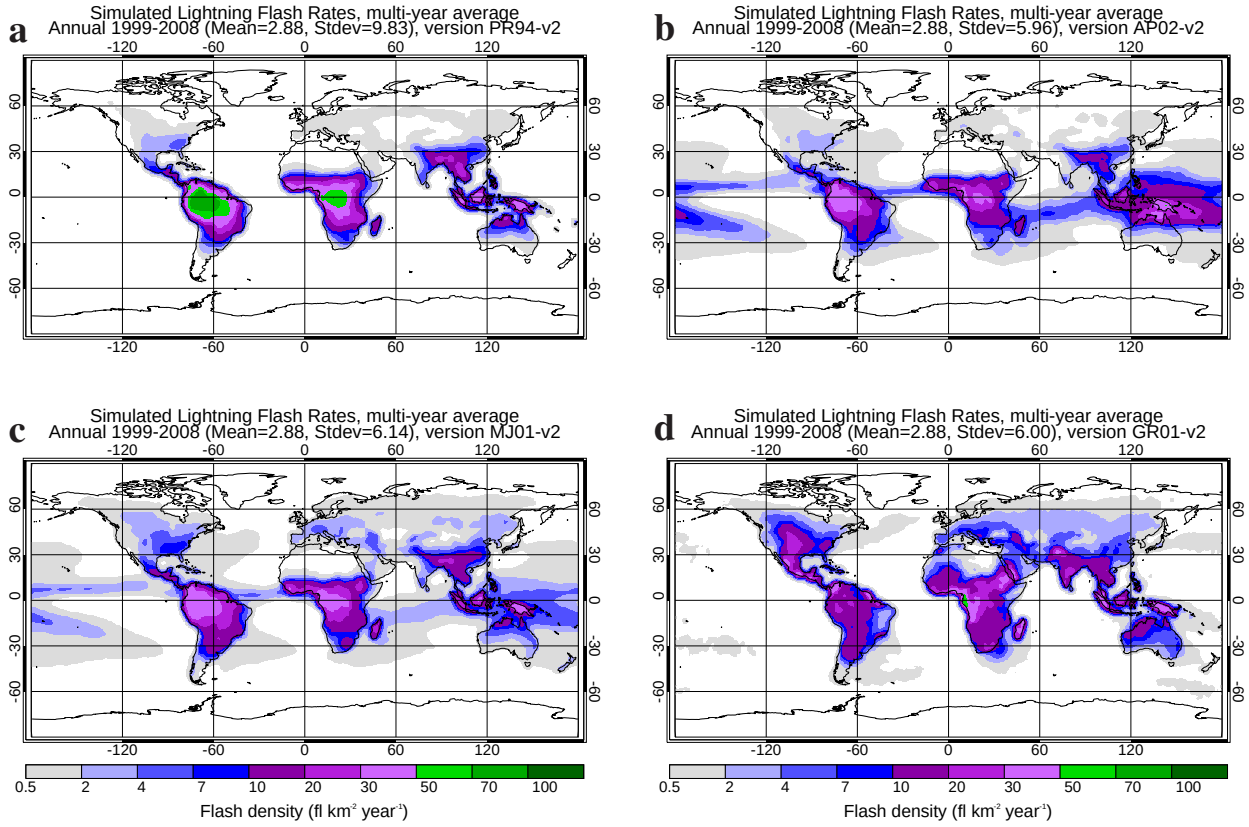

FIGURE 7: Annual mean lightning flash densities from the 1999-2008 year-long 80-km global simulations using the lightning parameterizations of (a) Price and Rind (1994), (b) Allen and Pickering (2002), (c) Meijer *et al.* 2001 and (d) Grewe *et al.* (2001). Flash densities are expressed in flashes km^{-2} $year^{-1}$. Global means and standard deviations are reported at the top of each panel. For comparison, similar plots for the new parameterization proposed in this study and for the LIS/OTD climatology are shown in Fig. 3.

Basin, too little over the extratropics and over the oceans and the standard deviation is strongly overestimated (9.83) compared to LIS/OTD (6.53). With AP02, lightning is overestimated over the Amazon Basin and tropical oceans while it is clearly underestimated in the extratropics and western India. MJ01 suffers from a slighter overestimation over tropical oceans and from a pronounced underestimation over the extratropics as well as over western India. Finally, the results from GR01 are those that agree the best with LIS/OTD as well as with the new parameterization, even though the standard deviation for GR01 (6.00) is further apart from the LIS/OTD value (6.53) than with the new parameterization (6.22). All these results confirm that the new paramaterization performs rather well.

5.2 Month-long simulations at various resolutions

In order to assess the sensitivity of the new lightning parameterization to horizontal resolution, a set of thirty-one 80-km, 25-km, and 9-km daily forecasts were run for the month of July 2012. As an illustration of the results, Fig. 8 displays the monthly mean lightning flash densities over the United States. It is clear that the results of the new parameterization exhibits a rather low sensitivity to horizontal resolutions, with just a slight increase from 20 to 24 flashes km^{-2} year^{-1} in mean lightning flash densities when resolution is varied from 80 km down to 9 km. Besides, field patterns look very similar across all three panels. This is a desirable behaviour which is partly attributable to the weak dependence of the outputs from the ECMWF convection scheme on horizontal resolution.

6 Adjoint sensitivity experiments

As a preliminary assessment of the future usefulness of the new lightning parameterization in the context of data assimilation, adjoint sensitivity experiments were carried out at a horizontal resolution of 50 km (model version 42r1). In this type of runs, the adjoint model is used to compute the sensitivities (or gradients) of a target criterion (valid at final time t_f) with respect to the model control vector, $\mathbf{x}$ (typically temperature, specific humidity, vorticity, divergence and surface pressure), several hours earlier (i.e. at initial time t_0). In other words, the sensitivities indicate how any given modification of the atmospheric state would change the value of the target criterion several hours later. In the example presented here, the target criterion, J_{ltg}, was defined as the simulated lightning flash density averaged between 2100 UTC 14 April and 0000 UTC 15 April 2012 inside a target geographical box centered over the central United States, as illustrated in Fig. 9. The target box encompasses a mesoscale convective system characterized by intense lightning acivity peaking above 5000 flashes km^{-2} year^{-1} on average over 3 hours.

In practice, a foreward integration is first performed with the (non-linear) forecast model, M, to determine J_{ltg} at final time t_f, which writes

$$\mathbf{x} \xrightarrow{M[t_0,t_f]} J_{ltg} = \frac{1}{N_t\, A_{box}} \sum_{t=1}^{N_t} \sum_{i=1}^{N_p} f_T(i,t)\; a_i\; \Phi_i \tag{6}$$

where N_t and N_p are the number of time steps and grid points to be averaged, respectively. Subscripts i and t denote grid point and time, respectively, while a_i is the area of each model grid box and A_{box} is the total area of the target box (i.e. the black box in Fig. 9). Φ_i is a smoothing function active near the edges of the target box (see Appendix 2), which prevents any noise coming from the handling of the discrete gradient of J_{ltg} in the spectral computations of the model ($\nabla_{f_T} J$ is only non-zero inside the target box).

The adjoint model, $\mathbf{M}^*$, is then initialized with the gradient of J_{ltg} with respect to lightning densities and is integrated backwards from time t_f to time t_0 to evaluate the sensivitities of J_{ltg} with respect to the

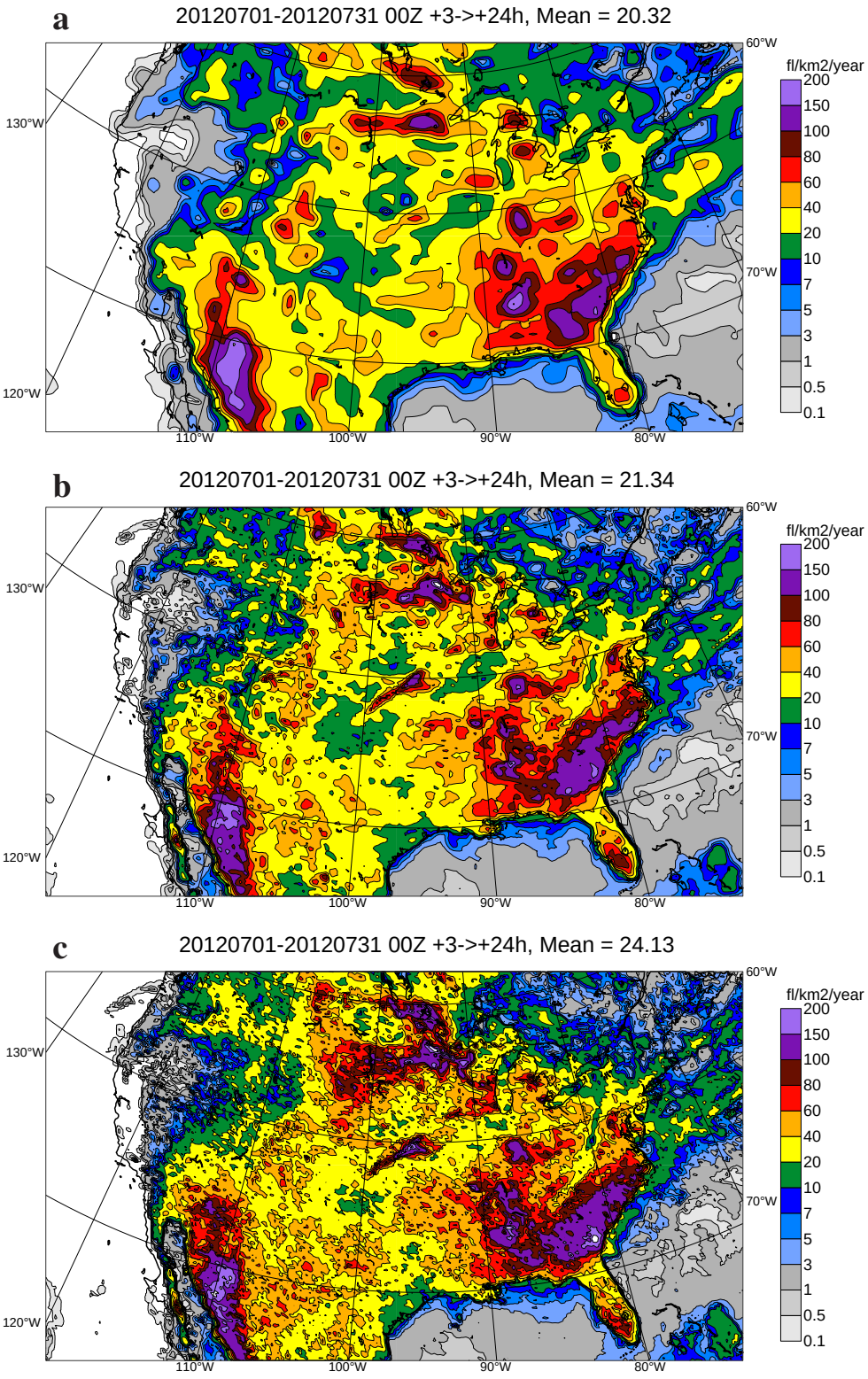

FIGURE 8: Mean lightning flash densities over the United States in July 2012 from global daily forecasts run at (a) 80-km, (b) 25-km and (c) 9-km horizontal resolution. Flash densities are expressed in flashes km^{-2} year^{-1}. The mean value over the plotted domain is reported at the top of each panel.

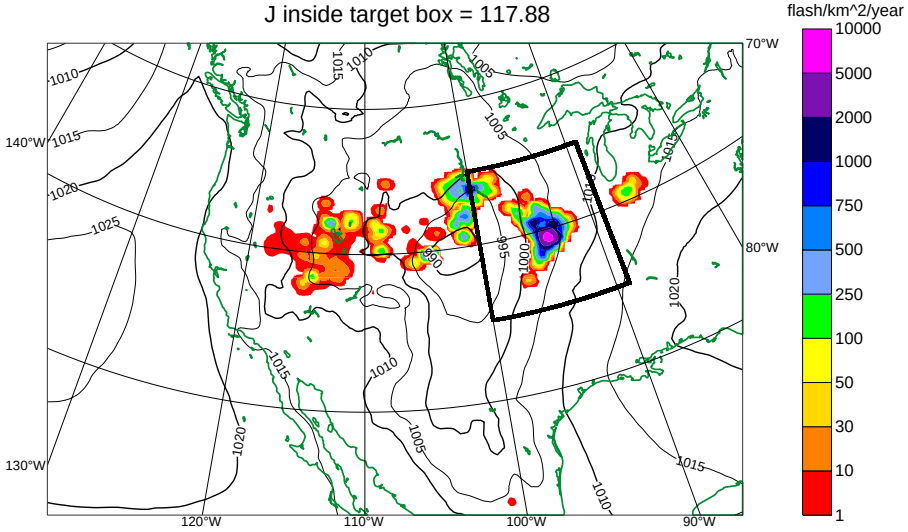

FIGURE 9: Simulated lightning flash densities (flashes km^{-2} year^{-1}) averaged over the period 2100 UTC 14 April and 0000 UTC 15 April 2012 over the United States, shown with colour shading. Mean-sea-level pressure (hPa) is also plotted with isolines. In sensitivity computations, the criterion of interest, J_{ltg}, was defined as the mean lightning flash density inside the target black box.

model control vector at initial time t_0. Formally, this can be written as

$$\left[\nabla_{f_T} J_{ltg}\right]_{t_f} = \frac{a_i\,\Phi_i}{N_t\,A_{box}} \xrightarrow{\mathbf{M}^*[t_f,t_0]} \left[\nabla_{\mathbf{x}} J_{ltg}\right]_{t_0} \tag{7}$$

One should stress here that the results from the adjoint approach are only reliable if the processes described in the model are not too far from linearity. In practice, at the resolution considered here, the linearized simplified code used in the ECMWF 4D-Var (Janisková and Lopez 2013) was shown to be a good approximation of the corresponding non-linear forecast model for integration lengths up to 24 hours (at least), even in convective situations.

In the case presented here, the value of J_{ltg} is equal to 117.88 flashes km^{-2} year^{-1}. Figure 10 displays maps of sensitivities of J_{ltg} to the model temperature, specific humidity and divergence at level 126 (approx. 400 m height) at 0000 UTC 14 April 2012, that is 24 hours before the validity time of J_{ltg}. Note that for convenience sensitivities have been scaled to a 100-m deep model layer. One can see that most of the sensitivities are located to the south-southwest of the target box, as expected given the prevailing background flow from the Gulf of Mexico at low levels (brown arrows). South of the target box, the strongest sensitivities are positive w.r.t. temperature and specific humidity and negative w.r.t. divergence. This indicates that a local heating or moistening or an increase in convergence at low-levels would lead to enhanced lightning activity inside the target box, 24 hours later. Such sensitivities make sense from a meteorological standpoint. Quantitatively, the maximum sensitivities to the selected three variables at the selected model level reach about 0.14 flash km^{-2} year^{-1} K^{-1}, 0.19 flash km^{-2} year^{-1} (g kg^{-1})$^{-1}$ and 1500 flashes km^{-2} year^{-1} s, respectively.

Figure 11 shows vertical cross-sections of sensitivities of J_{ltg} to temperature, specific humidity and divergence at 0000 UTC 14 April 2012 between points (25°N,100°W) and (40°N,95°W (black line in Fig. 10). These plots confirm that the highest sensitivities are confined well below 500 hPa, within the warm and humid flow from the Gulf of Mexico, and located upstream of the target box.

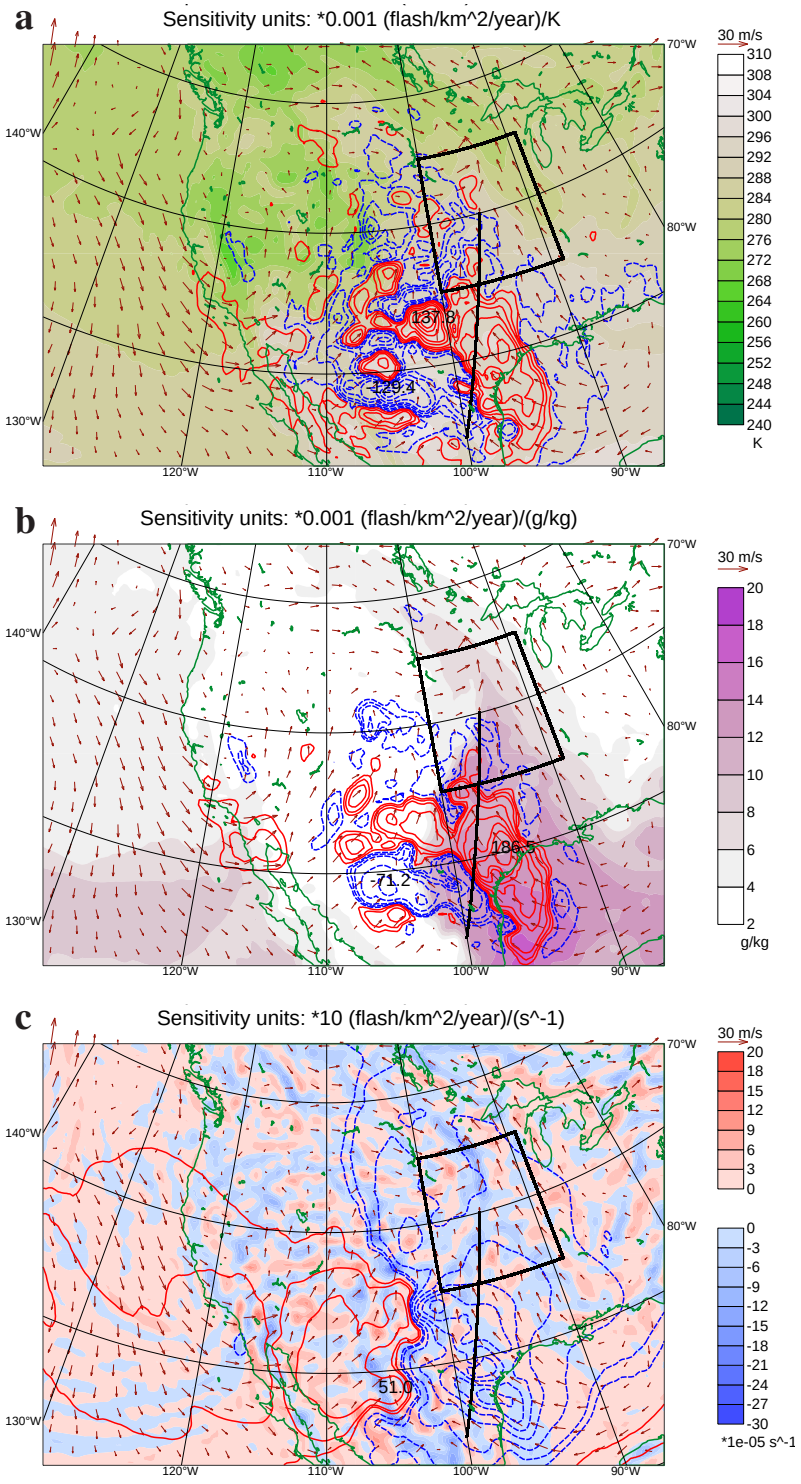

FIGURE 10: Maps of adjoint sensitivities (isolines) of the lightning criterion (J_{ltg}) to (a) temperature, (b) specific humidity and (c) divergence at z $\approx$ 400 m over the United States at 0000 UTC 14 April 2012, i.e. 24 hours prior to the validity time of J_{ltg}. Red (resp. blue) isolines correspond to positive (resp. negative) sensitivities. The units for sensitivities are given at the top of each panel. Note that sensitivities have been scaled to a 100-m deep model layer. Sensitivity contour absolute values are 1,5,10,20,30,50,75,100 in panel (a), 2,5,10,25,50,75,100,150,200 in (b) and 5,10,25,50,75,100,125,150,200 in (c). Colour shading displays the background field values (temperature, specific humidity or divergence), while brown arrows show the wind field at z $\approx$ 400 m (see legend on the side for scale and units). The black box indicates the target box where J_{ltg} is defined and the black tilted line shows the location of the cross-section displayed in Fig. 11.

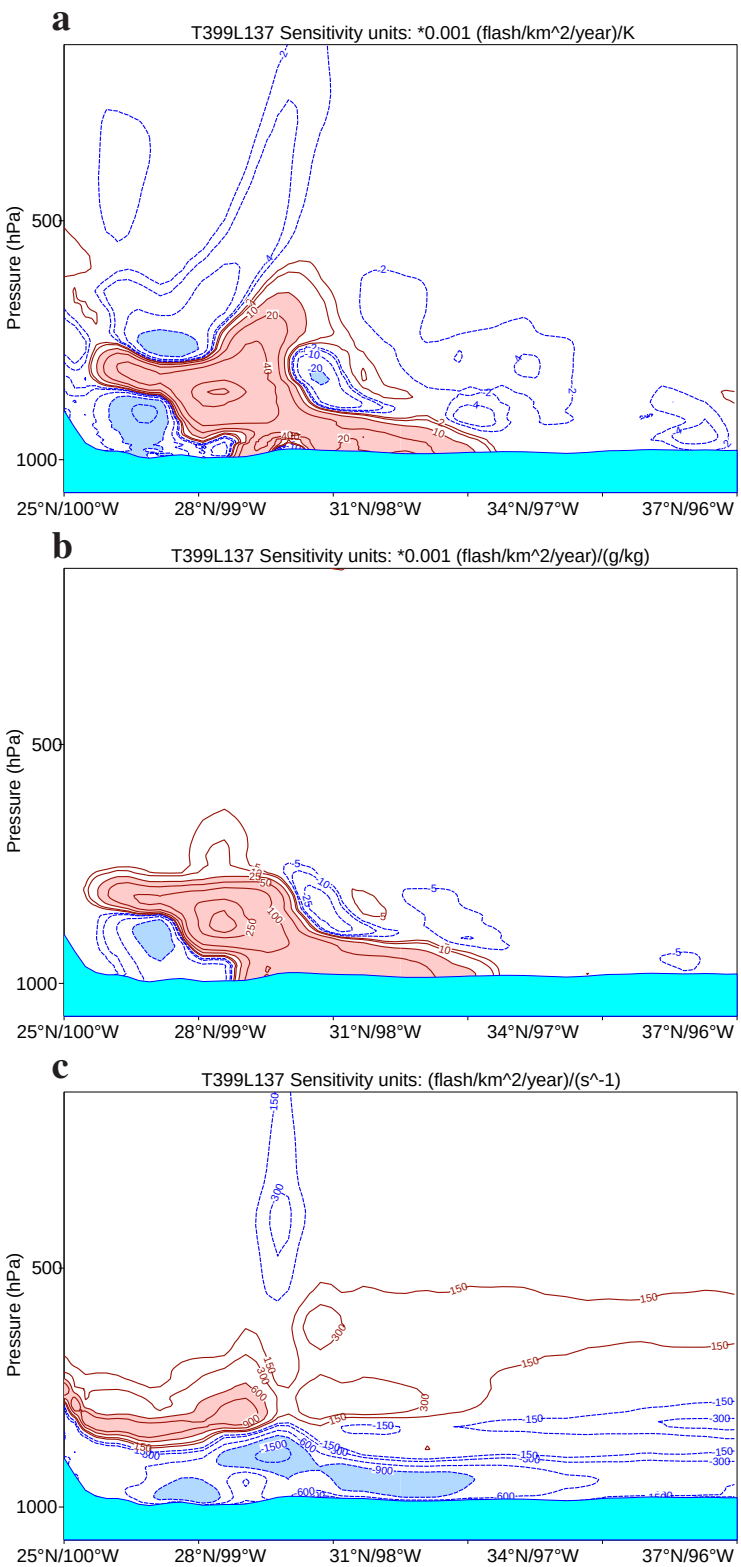

FIGURE 11: Vertical cross-section of adjoint sensitivities (isolines) of the lightning criterion (J_{ltg}) to (a) temperature, (b) specific humidity and (c) divergence at 0000 UTC 14 April 2012, i.e. 24 hours prior to the validity time of J_{ltg}. The cross-section extends between points (25°N,100°W) and (40°N,95°W), as shown in Fig. 10. The vertical coordinate is pressure (in hPa) and the cyan shading indicates the ground. Red (resp. blue) isolines correspond to positive (resp. negative) sensitivities. Sensitivity units are given at the top of each panel. Light red (resp. blue) shading highlights regions with stronger positive (resp. negative) sensitivities.

As an illustration of the results at higher levels, Fig. 12 displays the sensitivities of J_{ltg} to vorticity around 220 hPa. The series of dipole-shaped patterns over the West Coast suggests that lightning inside the target box could also be enhanced by strenghtening and straightening the meandering upper-tropospheric jet stream over that region.

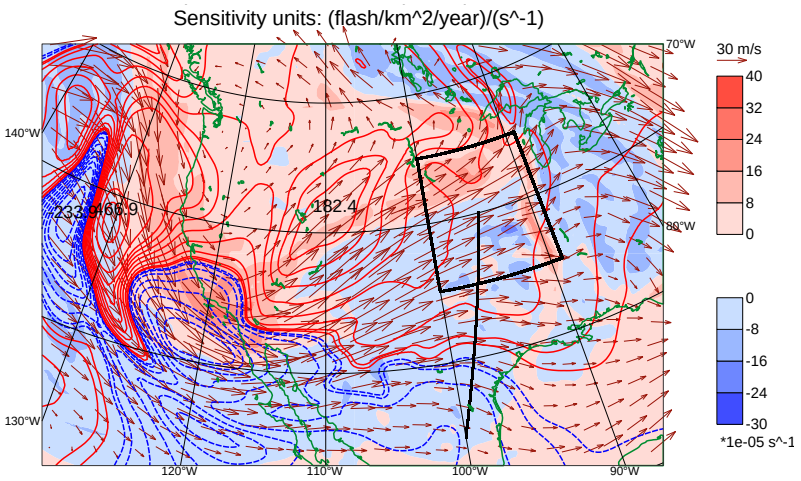

FIGURE 12: Same as in Fig. 10 but for adjoint sensitivities of J_{ltg} to vorticity around 220 hPa. Sensitivity contour absolute values are 5,10,25,50,75,100,125,150,200,300,400.

Overall, the experiment described in this section demonstrates that the adjoint version of the new lightning parameterization is able to produce meteorologically meaningful sensitivities of lightning to model prognostic variables a day earlier (at least). This result is encouraging for the prospect of assimilating lightning observations in the ECMWF 4D-Var system, since it suggests that it should be possible to successfully convert model−observation departures into increments of the model control variables at the beginning of the assimilation window. However, as highlighted in section 7, several other issues will need to be addressed before the assimilation of lightning data becomes a reality in the ECMWF 4D-Var.

7 Conclusions

A new parameterization able to diagnose lightning flash densities was developed for the ECMWF IFS, including its tangent-linear and adjoint versions. Lightning densities are expressed as a function of hydrometeors contents, convective available potential energy and cloud base height output by the convection scheme. Potential future applications range from the computation of NO_x emissions by lightning in a chemistry model, severe convective weather forecasting and data assimilation. In this study, a decade-long experiment was used to calibrate the global annual mean flash density against the LIS/OTD climatological value. On the seasonal timescale, the new parameterization agrees fairly well with LIS/OTD observations, even when individual continents are considered. In forecast mode, its results were found to be almost independent of horizontal resolution. Decade-long experiments also showed that the new parameterization gives better results overall than the main existing lightning parameterizations designed for global models. Sensitivity experiments using its adjoint version were also sucessfully performed as a preliminary assessment of its potential usage to assimilate lightning observations in the ECMWF 4D-Var system. For the latter purpose, however, the following important issues will need to be addressed:

(1) the quality of lightning observations (observation errors),

(2) the ambiguity of "no-lightning" observations (due to the detection threshold, potentially leading to biases in the analysis),
(3) the discrete nature of lightning in both time and space (background errors),
(4) the uncertainty about the physical processes involved (background errors),
(5) the temporal and spatial mismatch between simulated and observed lightning activity (particularly frequent when high-resolution and instantaneous data are considered).

Further revision of the lightning parameterization might be envisaged, should the representation of microphysical processes in the ECMWF model become more detailed, with the explicit calculation of graupel/hail contents for instance. Future efforts should also be devoted to parameterize cloud-to-ground (only) lightning activity so that model outputs can be compared with observations from ground-based networks, which mainly detect CG lightning. Over the few coming years, the next generation of geostationary satellites (GOES-R, 2016; MTG, 2019) will be equipped with lightning imagers (GLM, Goodman *et al.* 2013 and LI, Dobber and Grandell 2014, respectively). These instruments are expected to provide unprecedented temporal and spatial coverage with a resolution better than 10 km, thus nicely complementing ground-based networks and offering great potential for innovative applications in numerical weather and climate prediction.

Acknowledgements

Special thanks go to Peter Bechtold, Marta Janisková, Johannes Flemming, Anton Beljaars, Peter Bauer and Erland Källén of ECMWF for their early review of this manuscript. NASA Global Hydrology Resource Center should be acknowledged for providing access to the LIS/OTD lightning climatology (Cecil *et al.* 2014b).

APPENDIX 1

List of acronyms used in the text (alphabetical order)

ATDnet	=	Arrival Time Difference NETwork (UK).
ECMWF	=	European Centre for Medium-range Weather Forecasts.
ESA	=	European Space Agency.
EUMETSAT	=	EURopean organisation for the exploitation of METeorological SATellites.
GLDN	=	Global Lightning Detection Network (Vaisala).
GOES	=	Global Operational Environmental Satellite (NASA).
GLM	=	Geostationary Lightning Mapper (NASA).
LI	=	Lightning Imaging (EUMETSAT/ESA).
LINET	=	LIghtning detection NETwork (Europe).
LIS	=	Lightning Imaging Sensor (NASA).
MTG	=	MeteoSat Third Generation (EUMETSAT/ESA).
NASA	=	National Aeronautics and Space Administration (USA).
NLDN	=	National Lightning Detection Network (USA).
OTD	=	Optical Transient Detector (NASA).
TRMM	=	Tropical Rainfall Measuring Mission (USA).
WWLLN	=	World Wide Lightning Location Network (USA).

APPENDIX 2

Definition of the smoothing function Φ_i used in Eq. (6)

A filtering function Φ_i was applied to each grid point i inside the target box as seen in Eq. (6). This was meant to avoid the development of any potential noise during the adjoint sensitivity spectral computations, as a result of the discrete nature of J_{ltg}. Practically, Φ_i is defined as

$$\Phi_i = \left(\frac{1}{2}\right)^4 \left(1 - \cos\left(\pi \frac{\lambda_i - \lambda_w}{\Delta\lambda}\right)\right)\left(1 - \cos\left(\pi \frac{\lambda_e - \lambda_i}{\Delta\lambda}\right)\right)\left(1 - \cos\left(\pi \frac{\phi_i - \phi_s}{\Delta\phi}\right)\right)\left(1 - \cos\left(\pi \frac{\phi_n - \phi_i}{\Delta\phi}\right)\right) \tag{8}$$

where λ and ϕ denote longitude and latitude, respectively. Subscripts n, s, e, w stand for north, south, east and west and indicate the edges of the target box shown in Fig. 9. The values of $\Delta\lambda$ and $\Delta\phi$ determine the width of the outer region of the target box where the smoothing is applied. In the case described in section 6, $\Delta\lambda$ and $\Delta\phi$ were both set to 4 degrees. It should be noted that all arguments of the cosine in Eq. (8) are bounded between 0 and π. Eventually, Φ_i smoothly varies from 0 at the edges of the target box to 1 at its centre, as illustrated in Fig. 13.

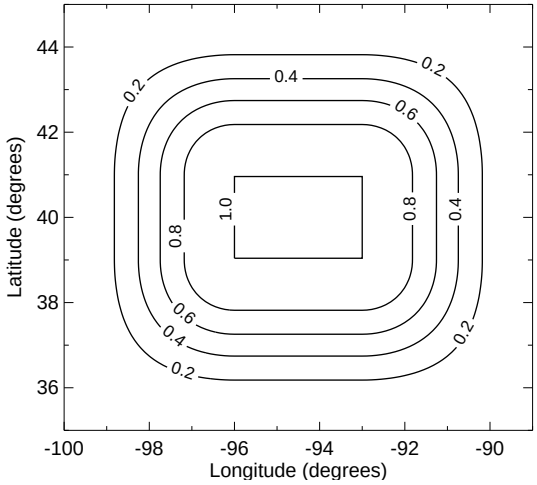

FIGURE 13: Filtering function Φ_i applied to the lightning criterion J_{ltg} in the adjoint sensitivity computations presented in section 6.

References

Allen, D. J. and Pickering, K. E. (2002). Evaluation of lightning flash rate parameterizations for use in a global chemical transport model. *J. Geophys. Res.*, 107. (D23), 4711, doi:10.1029/2002JD002066.

Anderson, G. and Klugmann, D. (2014). A European lightning density analysis using 5 years of ATDnet data. *Nat. Hazards Earth Syst. Sci.*, 14:815–829.

Barthe, C., Molinié, G., and Pinty, J.-P. (2005). Description and first results of an explicit electrical scheme in a 3D Cloud Resolving Model. *Atmos. Research*, 76:95–113.

Bechtold, P., Semane, N., Lopez, P., Chaboureau, J.-P., Beljaars, A., and Bormann, N. (2014). Representing equilibrium and non-equilibrium convection in large-scale models. *J. Atmos. Sci.*, 71:734–753.

Beirle, S., Koshak, W., Blakeslee, R., and Wagner, T. (2014). Global patterns of lightning properties derived by OTD and LIS. *Nat. Hazards Earth Syst. Sci.*, 14:2715–2726.

Betz, H. D., Schmidt, K., Laroche, P., Blanchet, P., Oettinger, W. P., Defer, E., Dziewit, Z., and Konarski, J. (2009). LINET - an international lightning detection network in Europe. *Atmos. Research*, 91:564–573.

Boccippio, D. J. (2002). Lightning Scaling Relations Revisited. *J. Atmos. Sci.*, 59:1086–1104.

Boccippio, D. J., Cummins, K. L., Christian, H. J., and Goodman, S. J. (2001). Combined Satellite- and Surface-Based Estimation of the Intracloud−Cloud-to-Ground Lightning Ratio over the Continental United States. *Mon. Weather Rev.*, 129:108–122.

Cecil, D. J., Buechler, D. E., and Blakeslee, R. J. (2014a). Gridded lightning climatology from TRMM-LIS and OTD: Dataset description. *J. Geophys. Res.*, 135-136:404–414.

Cecil, D. J., Buechler, D. E., and Blakeslee, R. J. (2014b). LIS/OTD/Gridded Lightning Climatology Data Collection Version 2.3.2014. NASA Global Hydrology Resource Center DAAC. http://doi.org/10.5067/LIS/LIS-OTD/DATA311.

Christian, H. J., Blakeslee, R. J., Boccippio, D. J., Boeck, W. L., Buechler, D. E., Driscoll, K. T., Goodman, S. J., Hall, J. M., Koshak, W. J., Mach, D. M., and Stewart, M. F. (2003). Global frequency and distribution of lightning as observed from space by the Optical Transient Detector. *J. Geophys. Res.*, 108. (D1), 4005, doi:10.1029/2002JD002347.

Christian, H. J., Blakeslee, R. J., and Goodman, S. J. (1989). The detection of lightning from geostationary orbit. *J. Geophys. Res.*, 94:13329–13337.

Christian, H. J. and co authors (1999). The Lightning Imaging Sensor. In *Proceedings of the 11th Conference on Atmospheric Electricity, Guntersville, AL, ICAE*, pages 746–749.

Chronis, T. G. and Anagnostou, E. N. (2003). Error analysis for a long-range lightning monitoring network of ground-based receivers in Europe. *J. Geophys. Res.*, 108. 4779, doi:10.1029/2003JD003776.

Courtier, P., Thépaut, J.-N., and Hollingsworth, A. (1994). A strategy for operational implementation of 4D-Var using an incremental approach. *Q. J. R. Meteorol. Soc.*, 120:1367–1388.

Dahl, J. M. L., Höller, H., and Schulmann, U. (2011). Modeling the Flash Rate of Thunderstorms. Part I: Framework. *Mon. Weather Rev.*, 139:3093–3111.

Dobber, M. and Grandell, J. (2014). Meteosat Third Generation (MTG) Lightning Imager (LI) Instrument Performance and Calibration from User Perspective. In *Proceedings of the 23rd Conference on Characterization and Radiometric Calibration for Remote Sensing (CALCON), 11-14 August 2014, Utah State University, Logan, Utah, USA*. 13 pages.

Fierro, A. O., Mansell, E. R., MacGorman, D. R., and Ziegler, C. L. (2013). The Implementation of an Explicit Charging and Discharge Lightning Scheme within the WRF-ARW Model: Benchmark Simulations of a Continental Squall Line, a Tropical Cyclone, and a Winter Storm. *Mon. Weather Rev.*, 141:2390–2415.

Finney, D. L., Doherty, R. M., Wild, O., Huntrieser, H., Pumphrey, H. C., and Blyth, A. M. (2014). Using cloud ice flux to parametrise large-scale lightning. *Atmos. Chem. Phys.*, 14:12665–12682.

Goodman, S. J., Blakeslee, R., Christian, H., Koshak, W., Bailey, J., Hall, J., McCaul, E., Buechler, D., Darden, C., Burks, J., Bradshaw, T., and Gatlin, P. (2005). The North Alabama Lightning Mapping Array: Recent severe storm observations and future prospects. *Atmos. Research*, 76:423–437.

Goodman, S. J., Blakeslee, R. J., Koshak, W. J., Mach, D., Bailey, J., Buechler, D., Carey, L., Schultz, C., Bateman, M., Jr., E. M., and Stano, G. (2013). The GOES-R Geostationary Lightning Mapper (GLM). *Atmos. Research*, 125-126:34–49.

Grewe, V., Brunner, D., Dameris, M., Grenfell, J. L., Hein, R., Shindell, D., and Staehelin, J. (2001). Origin and variability of upper tropospheric nitrogen oxides and ozone at northern mid-latitudes. *Atmos. Environ.*, 35:3421–3433.

Janisková, M. and Lopez, P. (2013). *Linearized physics for data assimilation at ECMWF*, volume II. Springer-Verlag Berlin Heidelberg. doi:10.1007/978-3-642-35088-7.

Kurz, C. and Grewe, V. (2002). Lightning and thunderstorms. Part I: Observational data and model results. *Meteor. Zeitschrift*, 11:379–393.

MacGorman, D. R. and Rust, W. D. (1998). Oxford University Press, Inc., New York. ISBN 0-19-507337-1, 422 pages.

Maggio, C. R., Marshall, T. C., and Stolzenburg, M. (2009). Estimations of charge transferred and energy released by lightning flashes. *J. Geophys. Res.*, 114. (D1), 4203, doi:10.1029/2008JD011506.

Mansell, E. R., MacGorman, D. R., Ziegler, C. L., and Straka, J. M. (2002). Simulated three-dimensional branched lightning in a numerical thunderstorm model. *J. Geophys. Res.*, 107. (D9), 4075, doi:10.1029/2000JD000244.

Meijer, E. W., van Velthoven, P. F. J., Brunner, D. W., Huntrieser, H., and Kelder, H. (2001). Improvement and Evaluation of the Parameterisation of Nitrogen Oxide Production by Lightning. *Phys. Chem. Earth*, 26:577–583.

Orville, R. E. and Huffines, G. R. (2001). Cloud-to-Ground Lightning in the United States: NLDN Results in the First Decade, 1989-98. *Mon. Weather Rev.*, 129:1179–1193.

Price, C. and Rind, D. (1994). Modeling Global Lightning Distributions in a General Circulation Model. *Mon. Weather Rev.*, 122:1930–1939.

Rabier, F., Järvinen, H., Klinker, E., Mahfouf, J.-F., and Simmmons, A. (2000). The ECMWF operational implementation of the four-dimensional variational assimilation. Part I: Experimental results with simplified physics. *Q. J. R. Meteorol. Soc.*, 126:1143–1170.

Rodger, C. J., Werner, S., Brundell, J. B., Lay, E. H., Thomson, N. R., Holzworth, R. H., and Dowden, R. L. (2006). Detection efficiency of the VLF World-Wide Lightning Location Network (WWLLN): Initial case study. *Ann. Geophys.*, 24:3197–3214.

Romps, D. M., Seeley, J. T., Vollaro, D., and Molinari, J. (2014). Projected increase in lightning strikes in the United States due to global warming. *Science*, 346:851–854.

Said, R. K., Inan, U. S., and Cummins, K. L. (2010). Long-range lightning geolocation using a VLF radio atmospheric waveform bank. *J. Geophys. Res.*, 115. D23108, doi:10.1029/2010JD013863.

Schumann, U. and Huntrieser, H. (2007). The global lightning-induced nitrogen oxides source. *Atmos. Chem. Phys.*, 7:3823–3907.

Stolz, D. C., Rutledge, S. A., and Pierce, J. R. (2015). Simultaneous influences of thermodynamics and aerosols on deep convection and lightning in the tropics. *J. Geophys. Res.*, 120. 6207-6231, doi:10.1002/2014JD023033.

Takahashi, T. (2006). Precipitation mechanisms in east Asian monsoon: Videosonde study. *J. Geophys. Res.*, 111. D09202, doi:10.1029/2005JD006268.

Vonnegut, B. (1963). Some facts and speculation concerning the origin and role of thunderstorm electricity. *Severe Local Storms, Meteor. Monogr.*, No. 27, Amer. Meteor. Soc., 224-241.

Williams, E. and Stanfill, S. (2002). The physical origin of the land-ocean contrast in lightning activity. *C. R. Physique*, 3:1277–1292.

Williams, E. R. and co authors (2002). Contrasting convective regimes over the Amazon: Implications for cloud electrification. *J. Geophys. Res.*, 107. (D20), 8082, doi:10.1029/2001JD000380.

Williams, E. R. and Sátori, G. (2004). Lightning, thermodynamic and hydrological comparison of the two tropical continental chimneys. *J. Atmos. Sol. Terr. Phys.*, 66:1213–1231. doi:10.1016/j.jastp.2004.05.015.